UDC 519.6 EDN: TJDWYY

NONLINEAR MODEL FOR DEFORMATION OF ADHERENT CELLS DUE TO SHEAR STRESS

N.A. Knyazev knyazev.n@icmm.ru
A.S. Nikityuk nas@icmm.ru

ICMM UB RAS, Perm, Russian Federation

Abstract

Phenotypic changes in cells are observed in many essential cellular processes. They are driven by external and internal stimuli of a biochemical and/or physical nature. To describe the mechanical behavior of cells under various loading conditions, numerous experimental methods are currently available. The primary difficulty in developing and investigating mathematical models using numerical simulation lies in several aspects. These include accounting for the evolution of the cell's internal structure, which directly influences its mechanical behavior, accurately describing the structural mechanisms and formulating constitutive relations with internal variables. In this study, we have performed numerical simulation of the process of instantaneous loading of a cell followed by a dwell using a statistical-thermodynamic model. The proposed model, formulated for small deformations, allows for the description of orientation mechanisms associated with actin filament behavior in a representative cell volume. Numerical results were compared with experimental data obtained via quantitative phase microscopy of cancer cells under shear stress conditions. An optimization problem was solved using the Nelder — Mead method to identify the model parameters. The evolution of the profile of the cytoskeleton's free energy is presented. The dependence of the potential barrier on the loading time was determined for different applied stress values

Keywords

Cell mechanical properties, quantitative phase microscopy, orientation mechanism, cancer cell

Received 02.07.2025
Accepted 19.01.2026

The work was carried out within the framework of a State Assignment (registration no. 124020200116-1)

Introduction. A range of significant cellular processes, including those contributing to pathological disease development, is critically associated with changes in cell phenotype. These changes manifest as alterations in cellular structure, mechanical properties, and the nature of cell interactions with the extracellular environment. For instance, epithelial-mesenchymal transition (EMT) leads to cell elongation, gene expression, reduced cell adhesion, and increased cell invasion, ultimately enabling mesenchymal cells to overcome dense layers of the extracellular matrix [1–3]. This transition is unequivocally important for the migratory behavior of normal cells in the context of wound healing and internal organ formation during human embryonic development [4, 5]. On the other hand, EMT mechanisms pose a significant challenge to the treatment of oncological diseases characterized by the metastasis of primary tumors to secondary sites [4, 6–8]. Phenotypic changes in cells are also observed in cancerous diseases and are accompanied by genetic mutations, cytoskeleton reorganization, and a reduction in the stiffness of cancer cells [9–11]. Ultimately, these factors determine the aberrant behavior of cancer cells, including uncontrolled proliferation, resistance to apoptosis, tumor initiation capacity, and metastatic potential [9, 12, 13].

Changes in cell phenotype are driven by a combination of external and internal stimuli, which can be biochemical and/or physical in nature. Mechanical forces are a key type of physical stimuli. These forces are generated by both external "passive" forces, which can originate from the surrounding environment, and internal "active" forces, driven by gene regulation and the reorganization of internal structures. Notable examples include experimental studies investigating the impact of mechanical stimuli on cell differentiation, such as cyclic stretching [14–16], cyclic compression [17], shear stress [18, 19], and microgravity [20–22]. In particular, [14] reports that cyclic stretching induces morphological and functional changes in osteosarcoma cells: elongation, increased surface area and roughness, and enhanced motility. An additional study [16] demonstrates that cardiomyocytes subjected to cyclic stretching exhibit elongation, accompanied by cytoskeletal reorganization and displacement of the cell nucleus towards one pole. Similar morphological alterations are observed in cells under cyclic compression. In [17] ovarian cancer cells were subjected to cyclic compression, leading to an increase in nuclear surface area and a reduction in cell circularity after recovery. A primary outcome of the structural changes was the appearance with disrupted actin structures in the cytoplasm, while highly stressed fibers were located at the cell membrane. The research in [18] investigates the response of endothelial cells to shear stress induced by laminar fluid flow, resulting in elongation and alignment of actin filaments with the flow direction, and an increase in cell cortical stiffness. The study in [19] argues that shear stresses initiated

by fluid flow promote breast cancer cell death and regulate tumor proliferation, but facilitate migration and metastasis of surviving cancer cells, while also increasing their adhesion, invasion, plasticity, and cell growth. More detailed information regarding the influence of fluid shear stress on cellular responses can be found in review articles [23, 24]. Microgravity can also trigger phenotypic changes in cells. Study [20] revealed reversible morphological and functional changes in MCF-7 breast cancer cells under microgravity, which manifested as two distinct cell phenotypes exhibiting differing proliferation and apoptosis rates. Reduced proliferation, adhesion, and migration of renal progenitor cells under simulated microgravity conditions were observed in [21], which was associated with disrupted F-actin cytoskeleton formation within the cells. A similar disorganization of the endothelial cell cytoskeleton exposed to weightlessness was reported in [22], accompanied by a decrease in the total number of actin filaments and microtubules. In addition to structural alterations, microgravity significantly reduced cell stiffness and viscosity and increased their circularity.

Understanding the patterns of cell response to external stimuli is crucial for comprehending the causes and development of various diseases according to specific scenarios. Modern methods for studying cellular responses allow for measuring mechanical properties and observing cell structure at the nanometer and piconewton scales. Atomic force microscopy (AFM) is a widely used method for studying the mechanical sensitivity of living cells [25, 26]. The operational principle of AFM relies on detecting the interaction between a probe and the cellular surface. This enables not only the examination of the cell surface, but also the evaluation of the nature of this interaction and the measurement of cellular mechanical properties with nanoscale sensitivity over a wide range of applied force. Quantitative phase microscopy (QPM) is another promising method for studying cell mechanics [27–29]. In contrast to AFM, QPM employs optical techniques to track cell dynamics, providing a non-invasive and contactless approach to biological monitoring. Furthermore, QPM allows for high-throughput analysis of cell populations, retaining nanoscale sensitivity. Other methods for studying cells include optical, acoustic, and magnetic tweezers, micropipette aspiration, substrate straining, microelectromechanical systems, and ultrasound stimulation [30].

To predict the mechanical behavior of cells in response to various external stimuli, mathematical models are developed and investigated that reflect the fundamental principles governing intracellular processes. Viscoelastic constitutive or structural-mechanical models represent the most significant class of models [31–34]. In these models, the viscoelastic behavior of cells is described using corresponding elastic (spring) and viscous (damper) elements connected

in series or parallel to form a single scheme. Each element within the scheme possesses its own material property parameter (Young's or shear modulus, viscosity) and should reflect the impact of individual components of the intracellular structure on the overall mechanical properties of the model. The model outcomes depend on the number of elements in the scheme, the type of element connections, and the values assigned to the viscosity and Young's (or shear) modulus parameters of the elements. Introducing a fractional element into the scheme leads to a nonlinear stress-strain relationship within power-law rheology models [35–39]. Varying the parameter of the fractional derivative (from 0 to 1) contributes to a change in the properties of the fractional element, enabling a transition from perfectly elastic to perfectly viscous behavior. Other classes of models also warrant consideration for describing cell mechanics, such as the soft glassy rheology model [40–44], a bio-chemo-mechanical model [45–48].

In the context of developing mathematical models, it is crucial to determine the mechanical properties of cells by considering the evolving internal structure, as this evolution directly affects cellular mechanical behavior. In the article [49], a statistical-thermodynamic model was developed to describe the mechanical properties of eukaryotic cells, considering orientation mechanisms related to actin filament ordering. The viscoelastic behavior of the cell is characterized by two elastic elements and one orientation element with a defined viscosity parameter of actin filament. It is worthwhile to validate these model representations using various types of mechanical experiments, such as an instantaneous loading protocol with a dwell, which can provide new insights into the evolution of the cell's internal structure. This knowledge could be valuable for understanding the fundamental basis of the development of pathological conditions.

This *study aims* to simulate the process of instantaneous cell loading followed by a dwell using the statistical-thermodynamic model, and to compare the simulation results with experimental quantitative phase microscopy data obtained from cancer cell subjected to shear stress. The article is structured as follows. The article describes an experimental setup for applying shear stress o breast cancer cells. The experiment aims to measure cell deformation under shear stress using quantitative phase microscopy The article also describes a mathematical model that describes the mechanical behavior of cells under instantaneous loading with a dwell. The article contains the main results of numerical simulations at different values of the applied load. The article compares and analyzes the numerical and experimental results concerning cell loading.

Quantitative phase microscopy for detecting cellular deformations. Quantitative phase microscopy presents a promising methodology for investigating the morphology, dynamics, and mechanical properties of biological

objects, such as DNA, cells, viruses, and cell monolayers. QPM provides the ability to perform non-invasive quantitative measurements of intracellular structures using low-intensity illumination. High-speed image acquisition enables the capture of biological processes and live cell dynamics in real-time, giving QPM unique advantages compared to other methods. Quantitative phase microscopy allows for the registration of spatial distributions of local optical path difference (OPD), also known as local phase difference or phase delay, introduced by optically transparent micro-objects.

Local OPD values of biological objects can be defined as

$$\phi(x, y) = \frac{2\pi}{\lambda}\left(n_{cell}(x, y) - n_{media}\right) d\left(x, y\right),$$

where λ is the wavelength; n_{cell} is the refractive index of the object; n_{media} is the refractive index of the surrounding medium; d is the cellular axial height. The optical capabilities of QPM allow for measuring phase delay at each point within a cell. Using this data, it is possible to calculate the object's geometry and measure its mechanical properties.

The study reported in [50] utilized QPM to investigate the mechanical properties of human colon, breast, lung, skin cancer cell lines. Shear stress generated by flowing surrounding medium was applied to cells adhered to the bottom of a rectangular channel flow cell. Data on the measured shear stress σ and phase delay $\varphi\left(x, y\right)$ were used to determine the shear modulus of a representative volume of a cell. The strain associated with that region was calculated according to the following algorithm.

A series of phase images of a cell were obtained during exposure to a given shear stress. From these images, the coordinates of the center of mass were calculated

$$x_C(t) = \frac{\sum\limits_{i,j,k} \varphi\left(t, x_i, y_j, z_k\right) x_i}{\sum\limits_{i,j,k} \varphi\left(t, x_i, y_j, z_k\right)}, \quad y_C(t) = \frac{\sum\limits_{i,j,k} \varphi\left(t, x_i, y_j, z_k\right) y_j}{\sum\limits_{i,j,k} \varphi\left(t, x_i, y_j, z_k\right)},$$

$$z_C(t) = \frac{\sum\limits_{i,j,k} \varphi\left(t, x_i, y_j, z_k\right) z_k}{\sum\limits_{i,j,k} \varphi\left(t, x_i, y_j, z_k\right)}.$$

Here x_C, y_C, z_C denote the coordinates of the center of mass of the cell's phase image. The magnitude of the displacement vector of the cell's phase image center of mass was determined as

$$\left|\mathbf{r}_C\left(t\right)\right| = \sqrt{\left(x_C(t)-x_C(0)\right)^2 + \left(y_C(t)-y_C(0)\right)^2 + \left(z_C(t)-z_C(0)\right)^2},$$

and cellular deformation was then estimated according to the relationship

$$\varepsilon^{expr}(t) = \frac{\left|\mathbf{r}_C(t)\right|}{h_e(t)}, \quad h_e(t) = \frac{\varphi\lambda}{2\pi\left\langle \Delta n \right\rangle},$$

where h_e is the cell height; Δn is the refractive index difference between a cell and the surrounding medium; $\langle \bullet \rangle$ indicates averaging. As shown in [50], the displacement primarily occurs along the x-axis, implying $\left|\mathbf{r}_C\right| \approx \Delta x$, where Δx is the displacement of the center of mass along the x-axis. Assuming small deformation, the shear modulus of a representative cell volume is calculated as follows:

$$G \approx \frac{\sigma}{\varepsilon^{expr}} \approx \frac{\sigma h_e}{\Delta x}. \tag{1}$$

As cells are inherently heterogeneous and anisotropic, it is important to emphasize that the measured shear modulus values were obtained exclusively for a representative volume of the cytoskeleton, based on the assumption of its homogeneity and isotropy. Figure 1 provides a schematic representation of the experiment involving the deformation of an adherent cell under shear stress.

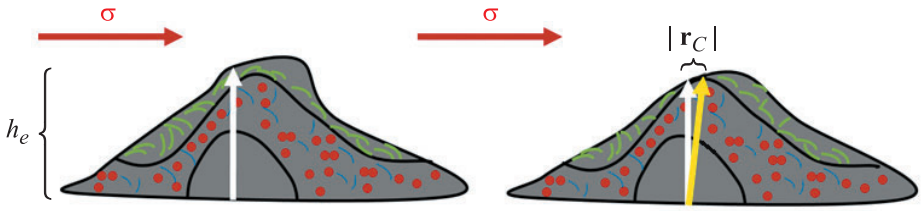

Fig. 1. Schematic representation of the experiment on the deformation of an adherent cell under the action of shear stress

The experiments demonstrated a strong correlation between the shear modulus and Young's modulus values of a representative volume of the cytoskeleton, obtained using quantitative phase microscopy and atomic force microscopy, respectively. Cell line samples were divided into three groups with different concentrations of an actin-depolymerizing toxin (0, 0.2, and 1 μM). Shear moduli (see Eq. (1)) and Young's moduli E were then determined using QPM and AFM. Specifically, at a zero concentration of the toxin, the average shear modulus values for cancer cells were 115 and 100 Pa, respectively. Assuming a Poisson's ratio of 0.5 for the cells, the relationship $E=3G$ was used to relate Young's modulus and the

shear modulus. It was observed that increasing the concentration of cytochalasin D led to a correlated decrease in both the shear modulus and Young's modulus, as measured by different methods. This highlights the considerable significance and prospective utility of quantitative phase microscopy in the context of cell mechanical property measurements. Its non-invasive nature, leading to minimal disruption of biological processes and the absence of damaging effects, enable it to sensitively detect structural and dynamic changes within cells.

These findings indicate that phase delay measurement techniques are promising tools for the investigation of the mechanics of living cells, taking into account their dynamically evolving internal structure. It is crucial, however, to have a model that directly accounts for the evolution of the internal structure. Therefore, the combination of QPM with such model representations has the potential to offer an effective approach for studying cell mechanical behavior, facilitating the development of new diagnostic tools and therapeutic strategies.

Mathematical model of representative cell volume based on statistical thermodynamics. A nonlinear mathematical model, employing the principles of statistical physics and linear thermodynamics, is proposed in [49] for the description of the mechanical behavior of eukaryotic cells. The model is formulated for small deformations, enabling the tracking structural changes and accounting for the influence of the evolving internal structure on the overall mechanical properties of the cell. A notable advantage of the model is the relatively small number of identifiable and verifiable parameters. Furthermore, numerical results from the model, describing deformation and stress relaxation processes in the cell, demonstrate good agreement with analogous results from fractional models.

A key feature of the model is its description of the orientation properties of the cell. For the purposes of modeling the behavior of an individual actin filament segment in three dimensions, a "microscopic" tensor is introduced:

$$\mathbf{s} = \frac{3}{4}\left(\mathbf{vv} - \frac{1}{3}\mathbf{I} \right), \tag{2}$$

where $\mathbf{v}$ is the unit vector along the segment axis; $\mathbf{I}$ is the unit tensor. In the transition to the macroscale, the tensor $\mathbf{s}$ is averaged over a small representative volume of the cell. The cell deformation tensor $\boldsymbol{\varepsilon}_o$, which reflects the orientation of the actin filaments, serves as a macroscopic order parameter and depends on the volume-averaged tensor $\mathbf{s}$ by the following expression:

$$\boldsymbol{\varepsilon}_o = N\gamma \left\langle \mathbf{s} \right\rangle = \frac{1}{2} N\gamma\eta \left(\mathbf{dd} - \frac{1}{3}\mathbf{I} \right), \tag{3}$$

where N signifies the volumetric concentration of these segments within the representative volume; γ represents the volume of an actin filament segment; $\mathbf{d}$ denotes the unit vector defining the direction of the applied force on the cell. The anisotropy parameter η in (3) characterizes the degree of order of the segments within the representative volume:

$$\eta = \frac{3}{2}\left\langle (\mathbf{v}\cdot\mathbf{d})^2 - \frac{1}{3}\right\rangle. \tag{4}$$

The parameter η ranges from – 0.5 to 1, where η = – 0.5 corresponds to a perpendicular arrangement of vectors $\mathbf{v}$ with respect to $\mathbf{d}$, $\eta = 1$ represents a parallel ordering of these vectors relative to $\mathbf{d}$, and $\eta = 0$ indicates an isotropic spatial distribution of the vectors $\mathbf{v}$. The resulting stress field acting on a single filament segment is then composed of external stresses $\boldsymbol{\sigma}_o$ and internal stresses associated with deformations $\boldsymbol{\varepsilon}_o$ during the remodeling of the actin cytoskeleton:

$$\mathbf{H} = \boldsymbol{\sigma}_o + \lambda\boldsymbol{\varepsilon}_o, \tag{5}$$

where λ is a parameter characterizing the stress field due to interactions between segments. Equation (5) allows for the determination of the orientation component of the actin filament segment energy, taking into account the traceless nature of tensors $\mathbf{H}$ and $\mathbf{s}$:

$$E = -\mathbf{H} : \gamma\mathbf{s} = -\left(\boldsymbol{\sigma}_o + \lambda\boldsymbol{\varepsilon}_o\right) : \gamma\mathbf{s}. \tag{6}$$

To establish different orientation states of a system with energy E, the Boltzmann — Gibbs distribution is used. Within this framework, each actin filament segment is considered a quasi-closed system — a part of a closed system, in which the energy of interaction with other parts of the system is negligible [51]. The probability W of a state of an individual subsystem, when the orientation component of energy takes the value E, is calculated using the relation:

$$W(E) = \left(\int_{\Omega} \exp\left(-\frac{E}{\theta}\right) d\Omega\right)^{-1} \exp\left(-\frac{E}{\theta}\right), \tag{7}$$

where θ is the effective temperature factor; Ω is the phase space of possible segment orientation. The deformation tensor ε_o, which describes orientation effects within the entire system (representative volume of the cell), is determined by employing Eq. (7):

$$\boldsymbol{\varepsilon}_o = N\int_{\Omega} \gamma\mathbf{s}\, W d\Omega. \tag{8}$$

Equations (2)–(8) form a closed system, which reduces to the self-consistence equation. Under conditions of simple shear loading, the expressions for the deformations and stresses are given by

$$\boldsymbol{\sigma}_o = \frac{\sigma_o}{2}\left(\mathbf{id}+\mathbf{di}\right),\ \ \boldsymbol{\varepsilon}_o = \frac{\varepsilon_o}{2}\left(\mathbf{dd}-\frac{1}{3}\mathbf{I}\right), \tag{9}$$

where σ_o, ε_o represent the magnitudes of the shear stress and orientational deformation, respectively; $\mathbf{i}$ is the unit vector along the normal to the plane of shear. Since the orientational deformation under shear loading is defined by a single value ε_o, the one-dimensional form of the self-consistency Eq. (8) may be considered to simplify the determination of $\varepsilon_o / 2$ from (9):

$$\varepsilon'_o = \frac{\int_0^1 \frac{3}{2}\left(z^2-\frac{1}{3}\right)\exp\left(\frac{3}{4}\left(\sigma'_o+\chi_o^{-1}\varepsilon'_o\right)\left(z^2-\frac{1}{3}\right)\right)dz}{\int_0^1 \exp\left(\frac{3}{4}\left(\sigma'_o+\chi_o^{-1}\varepsilon'_o\right)\left(z^2-\frac{1}{3}\right)\right)dz}. \tag{10}$$

Here $\sigma'_o, \varepsilon'_o$ are dimensionless scalar values corresponding to the non-zero components of the tensors $\boldsymbol{\varepsilon}_o$ and $\boldsymbol{\sigma}_o$ in the one-dimensional case; z is the projection of the filament segment orientation vector onto the shear direction ($z = \mathbf{v}\cdot\mathbf{d}$), $\chi_o = \theta/(\lambda\gamma)$. The derivation of Eq. (10) also involved the non-dimensionalization of the model parameters $s' = \gamma N s$, $\varepsilon'_o = \varepsilon_o$, $\sigma'_o = (\gamma/\theta)\sigma_o$ (dimensionless quantities are indicated by prime).

A substitution $\xi = \sigma'_o + \chi_o^{-1}\varepsilon'_o$ allows the self-consistency Eq. (10) to be expressed as a functional dependence $\varepsilon'_o(\xi)$. An approximation for the inverse relationship $\xi(\varepsilon'_o)$ takes the form

$$\xi = \frac{260+\varepsilon'_o\left(123\,200+\left(76\,250-114\,200\,\varepsilon'_o\right)\varepsilon'_o\right)}{0.124+\varepsilon'_o\left(0.1677+\varepsilon'_o\left(-0.2067+\left(-0.0882+\varepsilon'_o\right)\varepsilon'_o\right)\right)}. \tag{11}$$

This relation was obtained through an analytical solution of Eq. (10). Expressions (10), (11) provide a pathway to determining the nonlinear function $w(\varepsilon_o)$, responsible for the orientation effects within the model:

$$w\left(\varepsilon'_o\right) \equiv \frac{\partial F'}{\partial \varepsilon'_o} = \sigma'_o = \xi\left(\varepsilon'_o\right) - \chi_o^{-1}\varepsilon'_o, \tag{12}$$

where $F' = (\gamma F)/\theta$, with F representing the Helmholtz free energy. In terms of the thermodynamic potential $\Psi(\varepsilon_o, \sigma_o) = F(\varepsilon_o) - \sigma_o\varepsilon_o$ Eq. (12) is transformed into

$$\frac{\partial \Psi'}{\partial \varepsilon'_o} = \xi\left(\varepsilon'_o\right) - \chi_o^{-1}\varepsilon'_o - \sigma'_o.$$

In addition to the description of the orientation properties of actin filaments, the proposed statistical-thermodynamic model reflects the viscoelastic characteristics of other structural components of the cell. To model the properties of structural elements and determine the relationship between them, the representative volume of the cell is represented by a structural-mechanical analogue, allowing for an adequate description of the behavioral characteristics of the representative volume. The scheme of the model consists of an elastic element, responsible for the reversible deformation of the entire system, and a Maxwell-type element, connected in parallel. The Maxwell-type element, in turn, comprises a series connection of an elastic element and an orientation element, characterizing the elastic and orientation properties of actin filament segments within the cell, respectively. The transition from Young's moduli to shear moduli G_r and G_e is achieved through the following relation $E = 3G$, derived from the relationship for an isotropic elastic material with $\nu = 0.5$, analogous to the work presented in [52].

The constitutive relation for the proposed model was obtained by solving the system of evolutionary equations for the cell's representative volume, utilizing the framework of linear thermodynamics. The system satisfies the thermodynamic principles. The thermodynamic potential F was assumed to be a function of the parameters $\varepsilon, \varepsilon_e, \varepsilon_o$ and T, thus depending on elastic $\left(\varepsilon_e = \varepsilon - \varepsilon_o\right)$, orientation $\left(\varepsilon_o\right)$, and thermal ($T$) effects. Throughout the development of the system, Onsager's theorem was also applied, and a hypothesis of a linear relationship between thermodynamic forces and fluxes was proposed. The final form of the constitutive relation on the one-dimensional case under simple shear, neglecting large temperature gradient changes and non-local effects, is given by

$$\frac{\nu_o}{3G_e}\frac{d\sigma}{dt} + \sigma = \nu_o \frac{G_r + G_e}{G_e}\frac{d\varepsilon}{dt} + 3G_r\varepsilon + w\left(\varepsilon_o\right), \tag{13}$$

where ν_o is the viscosity coefficient of the orientation element; G_r, G_e are the shear moduli of the elastic elements; σ is the shear stress; ε is the shear strain. Equation (13) exhibits a strong resemblance to the constitutive relation of the standard linear solid viscoelastic model [53], with the exception of the nonlinear term $w(\varepsilon_o)$, which describe the orientation properties within the cell's representative volume. In the numerical experiment involving instantaneous loading

with a dwell the shear stresses remain constant; therefore, the resulting form of the constitutive relation is

$$\frac{d\varepsilon}{dt} = \frac{1}{\nu_o}\frac{G_e}{G_r + G_e}\left(\sigma - 3G_r\varepsilon - w\left(\varepsilon_o\right)\right). \tag{14}$$

The viscosity coefficient of the orientation element in (14) is calculated using the following expression: $\nu_o = 3G_e\tau_o \exp\left(\Delta\Psi'\right)$, where τ_o is the period of the natural oscillations of the actin filament segments; $\Delta\Psi'$ is the magnitude of the potential barrier that the system must overcome to orient all segments within the cell's representative volume in a specific direction.

In this manner, the addition of initial conditions to Eq. (14) yields a closed system that enables the simulation of the response of the cell's representative volume to an applied shear deformation.

Numerical simulation of adherent cell deformation under shear loading. To evaluate the relevance of the proposed mathematical model of the cell, a series of numerical experiments simulating the loading process of the cell's representative volume were conducted. The presence of unknown parameters in the model necessitated a distinct stage of work to identify and verify these parameters using experimental data [50] acquired under conditions of instantaneous loading followed by a dwell.

Figure 2 presents a comparison of experimental and numerical results for the change in total strain over time at various shear stress values. The numerical results exhibit good agreement with the experimental data in both linear (Fig. 2, *a*) and logarithmic (Fig. 2, *b*) scales. For quantitative comparison, the maximum relative error was calculated for each numerical solution using the following formula:

$$W = \max_{i=1,n}\left(\left|\frac{\varepsilon_i^{expr} - \varepsilon_i^{num}(\mathbf{x})}{\varepsilon_i^{expr}}\right|\right)\cdot 100\ \%, \tag{15}$$

where $\varepsilon_i^{\exp r}, \varepsilon_i^{num}$ denote the experimental and numerical values of the total deformation at time t_i, respectively. The vector of identifiable model parameters $\mathbf{x}$ in (15) consists of five components: the shear moduli G_r, G_e, the orientation property parameters of the cell λ and γ, and the period of the natural oscillations of the actin filament segments τ_o. These parameters were determined by solving an optimization problem, specifically minimizing the functional

$$S = \sqrt{\sum_{i=1}^{n}\left(\frac{\varepsilon_i^{expr} - \varepsilon_i^{num}(\mathbf{x})}{\varepsilon_i^{expr}}\right)^2} \to \min.$$

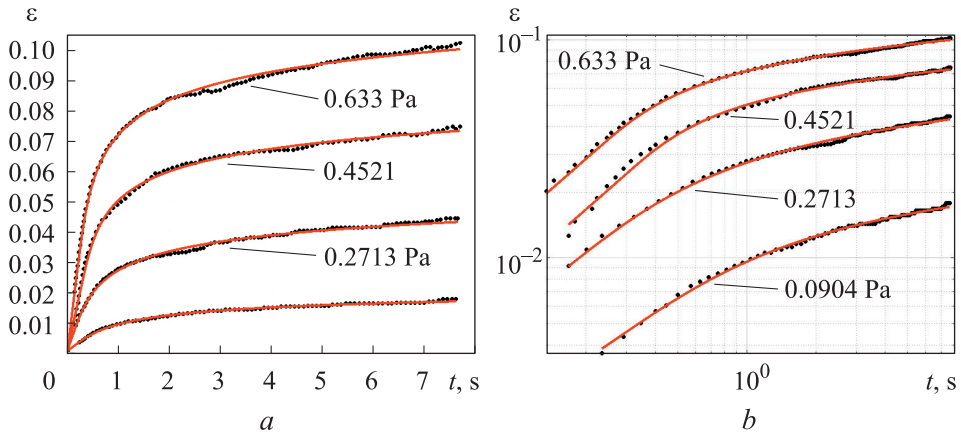

Fig. 2. Experimental (black dots) and numerical (red solid lines) plots illustrating the dependence of total deformation on time, shown in linear (*a*) and logarithmic (*b*) scales

Maximum relative error of numerical solutions with characteristic shear stress σ, Pa, following:

	0.633	0.4521	0.2713	0.0904
W, %	10.7	12.5	6	5.3

As a result, the values of the parameters $G_r, G_e, \lambda, \gamma, \tau_o$ were computed for each curve corresponding to a specific shear stress σ (with θ assumed to be $310\,k_B J$, where k_B is the Boltzmann constant). The mean value and the standard deviation of these parameters, based on four curves, are presented below:

G_r, Pa ..... 3.44 ± 0.83
G_e, MPa ..... 12.7 ± 4.6
λ, Pa ..... 0.9 ± 0.49
γ, m^3 ..... $(7.45 \pm 3.59) \cdot 10^{-19}$
τ_o, s ..... $(4.74 \pm 1.76) \cdot 10^{-7}$

The value of the total deformation ε at the unloading point demonstrates a linear dependence on the magnitude of the applied stress in the model (Fig. 3). This indicates that the cells indeed exhibit linear viscoelastic properties, and the assumption of small deformations is adequate.

Using the identified model parameters corresponding to the curve with a shear stress of σ = 0.633 Pa (see Fig. 2), graphical representations of the total deformation $\varepsilon = \varepsilon_o + \varepsilon_e$ and its components ε_o and ε_e as a function of the loading time were constructed (Fig. 4, *a*). The figure shows that the orientation

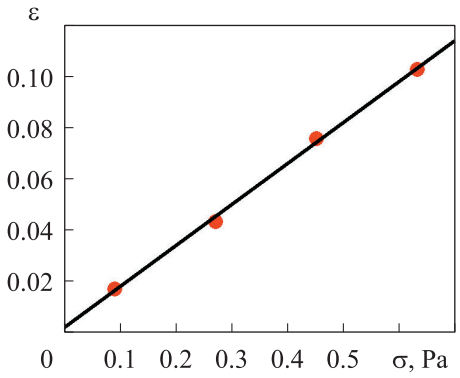

component of deformation ε_o closely approaches the magnitude of the total deformation ε throughout the entire loading period, while its elastic component ε_e remains negligibly small.

Fig. 3. Total deformation at unloading versus applied stress (red dots) and its linear approximation (black solid line)

Analogous plots showing the total stress $\sigma = \sigma_o + \sigma_r$ and its components σ_o, σ_r are presented in Fig. 4, *b*. The stress components σ_o, σ_r mutually compensate to maintain the total stress σ constant at 0.633 Pa throughout the loading period.

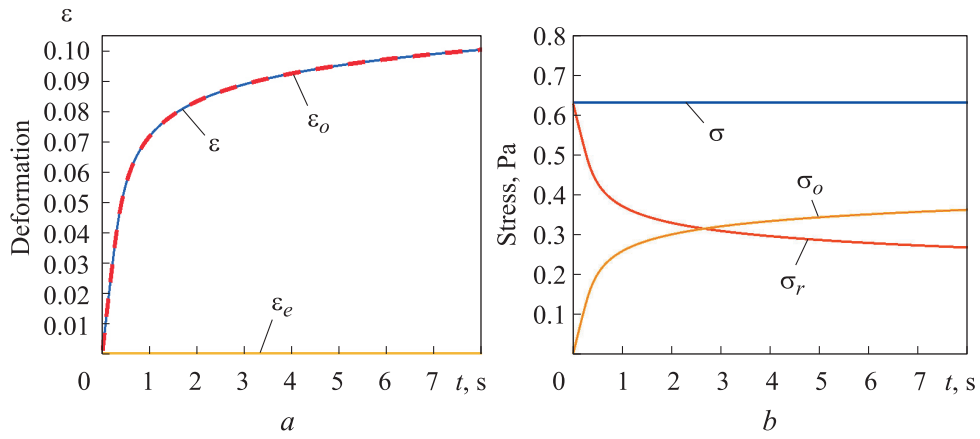

Fig. 4. Dependence of deformations ε, ε_o, ε_e (*a*) and stresses σ, σ_o, σ_r (*b*) on loading time

A distinctive feature of the statistical-thermodynamics model of the cell, defining its potential, it the ability to analyze the orientation process of the cytoskeleton filament segments. Figure 5, *a* illustrates the profiles and instantaneous values of free energy, used to calculate the viscosity of the orientation element in the model, at times t = 0, 0.4, and 5 s. The instantaneous value of Ψ is determined both by the magnitude of the stress σ_o, affecting the profile curve's shape, and by the deformation ε_o, defining a specific point on that curve. As the loading time increases, the stress σ_o decreases (see Fig. 4, *b*), which is accompanied by a decrease in the slope of the profile. A longer loading period also leads to growth in the deformation ε_o, which influences the movement of the point

characterizing the instantaneous value of the thermodynamic potential Ψ in the positive direction.

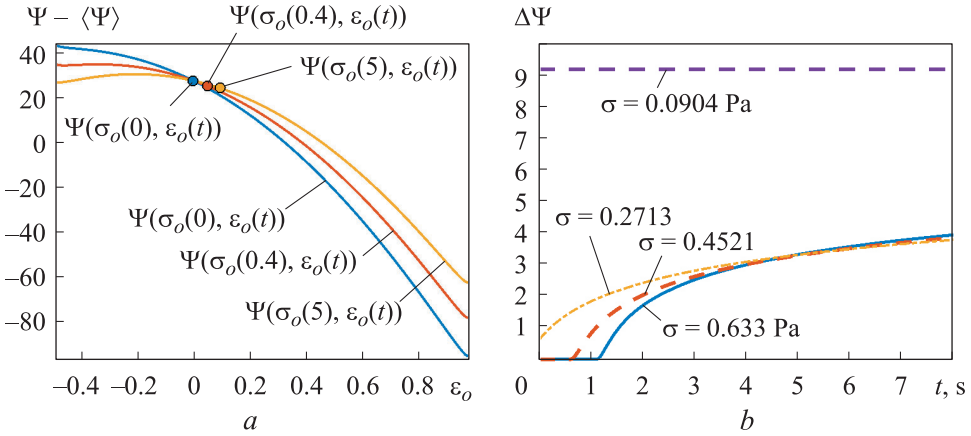

Fig. 5. Profiles and instantaneous values of the thermodynamic potential Ψ at times $t = 0$, 0.4 and 5 s (*a*), potential barrier height as a function of loading time for different applied stress levels (*b*)

The dependence of the potential barrier height $\Delta\Psi$ on the loading time for various values of the applied stress is depicted in Fig. 5, *b*. The energy barrier height continuously rises with lengthening loading time. Increasing the applied stress σ greatly affects the significant quantitative changes in $\Delta\Psi$. Specifically, during the initial loading phase, the magnitude of the potential barrier $\Delta\Psi$ decreases with increasing σ, thereby facilitating the transition of the system between various states. At $\sigma = 0.0904$ Pa, a sharp rise in the potential barrier height is observed, followed by a negligible subsequent growth throughout the loading period.

Discussion. This study investigates the mechanical response of cells under instantaneous loading followed by a dwell, using a statistical-thermodynamic model that incorporates the orientation properties of the cell cytoskeleton. The development of new methods and mathematical models for studying cell function at different stages of human life is driven by the necessity of accounting for alterations in cell structural features to determine their physical and biochemical properties. To describe the mechanical behavior of cells, a theoretical approach was employed, based on self-consistent field methods and quasi-equilibrium thermodynamics. The sufficiency of the numerical results was evaluated through comparison with experimental data derived from an investigation of the mechanical properties of cells using QPM under shear stress.

A fundamental aspect of the cell model in this study is the description of the viscoelastic properties of filament segments and their collective behavior within

a representative volume, as well as the interactions between these components. The structural-mechanical scheme and the constitutive relation of the model exhibit a significant similarity to those of the standard linear solid model [53]. A distinctive feature of the considered model is its nonlinearity, which is attributed to the necessity of accounting for the mechanism of inelastic deformation associated with the orientation of actin filament segments. To describe orientation effects, an order parameter was introduced into the model, analogous to the approach in [54], where orientation mechanisms were considered in the context of rigid polymer. The calculation of the orientation element's viscosity involves a continuous spectrum of stress relaxation, which changes dynamically and depends on the structural parameters. This allows for the description of multiple relaxation processes in cells and significantly reduces the number of model parameters.

Numerical modeling was performed to simulate the process of instantaneous loading of a representative cell volume followed by a dwell. Creep behavior was observed under the specified loading conditions. The model parameters were identified based in experiments [50]. A comparison of the numerical and experimental data for shear strain as a function of loading time showed good agreement in both linear and logarithmic scales. The maximum relative error for the stress levels 0.633, 0.4521, 0.2713, and 0.0904 Pa was 10.7, 12.5, 6, and 5.3 %, respectively. The mean value and standard deviation for each model parameter were then calculated using the four curve sets.

An analysis was performed to define how the deformation at unloading depends on the magnitude of the applied shear stress within the model. A linear relationship between these parameters was confirmed, indicating a linear viscoelastic behavior and agreeing well with the assumption of small deformations in the model. The time-dependent behavior of the strains ε, ε_o, and ε_e and stresses σ, σ_o, and σ_r was illustrated graphically. Numerical simulations performed at $\sigma = 0.633$ Pa revealed a significant contribution of the orientation strain component ε_o to the total strain ε. The extremely small deformation ε_e arises from the large elastic modulus G_e of the Maxwell-type element, suggesting that the orientation mechanism dominates over the elastic mechanism in describing the deformation of actin filaments in the model. The analysis of the time-dependent stress profiles $\sigma(t)$, $\sigma_o(t)$, and $\sigma_r(t)$ confirmed that the total stress remained constant. Profiles and instantaneous values of the thermodynamic potential Ψ, depending on the parameters ε_o and σ_o, were illustrated at various time points. The variation in Ψ during loading result from both the transformation of the profile curve's shape and the movement of the point, rep-

resenting the instantaneous value of Ψ, along the specified curve. The barrier height $\Delta\Psi$, calculated from the shape of the free energy profile, continuously increases throughout the loading process. Variations in the magnitude of the applied external shear stress have a significant impact on the value of $\Delta\Psi$.

The presented mathematical model of the cell allows for the description of purely mechanical effects on the cell cytoskeleton, which constitutes a limitation of the model. To understand native morphological and functional changes in cells during various cellular processes, it is necessary to consider the influence of biochemical and physical (non-mechanical) stimuli. Furthermore, the current model primarily focuses on the deformation mechanisms of actin filament segments within the cell, while the role of other structural elements in the cells mechanical response remains unclear. This highlights a potential direction for further model development by incorporating other mechanisms and their carriers, such as Ca^{2+} ion diffusion (responsible for actin filament polymerization and depolymerization), other chemical signals, microtubules, intermediate filaments, the plasma membrane, or the nucleus. This incorporation can be achieved by defining appropriate internal variables and constitutive relations for them.

Conclusion. A numerical simulation was performed to investigate the response of a cell to instantaneous loading followed by a dwell, utilizing a statistical-thermodynamic model that incorporates the orientational properties of the cell's cytoskeleton. The model parameters were identified, demonstrating strong concordance between numerical and experimental data in both linear and logarithmic scales. A linear relationship was confirmed between deformation at unloading and the magnitude of the applied shear stress, indicating a linearly viscoelastic deformation behavior. The temporal evolution of deformations ε, ε_o, ε_e, and stresses $\sigma, \sigma_o, \sigma_r$ was plotted, revealing a creep phenomenon under the specified loading conditions. The variation of the potential Ψ and the barrier height $\Delta\Psi$ with respect to parameters ε_o, σ_o, and σ was demonstrated.

REFERENCES

[1] McGrail D.J., Mezencev R., Kieu Q.M.N., et al. SNAIL-induced epithelial-to-mesenchymal transition produces concerted biophysical changes from altered cytoskeletal gene expression. *FASEB J.*, 2015, vol. 29, iss. 4, pp. 1280–1289. DOI: https://doi.org/10.1096/fj.14-257345

[2] Sullivan E., Harris M., Bhatnagar A., et al. Boolean modeling of mechanosensitive epithelial to mesenchymal transition and its reversal. *IScience*, 2023, vol 26, iss. 4, art. 106321. DOI: https://doi.org/10.1016/j.isci.2023.106321

[3] Christiansen J.J., Rajasekaran A.K. Reassessing epithelial to mesenchymal transition as a prerequisite for carcinoma invasion and metastasis. *Cancer Res.*, 2006, vol. 66, iss. 17, pp 8319–8326. DOI: https://doi.org/10.1158/0008-5472.CAN-06-0410

[4] Kim D.H., Xing T., Yang Z., et al. Epithelial mesenchymal transition in embryonic development, tissue repair and cancer: a comprehensive overview. *J. Clin. Med.*, 2018 vol. 7, no. 1, art. 1. DOI: https://doi.org/10.3390/jcm7010001

[5] Thiery J.P., Acloque H., Huang R.Y.J., et al. Epithelial-mesenchymal transitions in development and disease. *Cell*, 2009, vol. 139, iss. 5, pp. 871–890.
DOI: https://doi.org/10.1016/j.cell.2009.11.007

[6] Yang B.W., Bai J., Shi R., et al. TGFB2 serves as a link between epithelial-mesenchymal transition and tumor mutation burden in gastric cancer. *Int. Immunopharmacol.*, 2020, vol. 84, art. 106532. DOI: https://doi.org/10.1016/j.intimp.2020.106532

[7] Wu Y., Zhou B.P. New insights of epithelial-mesenchymal transition in cancer metastasis. *Acta Biochim. Biophys. Sin.*, 2008, vol. 40, iss. 7, pp. 643–650.
DOI: https://doi.org/10.1111/j.1745-7270.2008.00443.x

[8] Ang H.L., Mohan C.D., Shanmugam M.K., et al. Mechanism of epithelial-mesenchymal transition in cancer and its regulation by natural compounds. *Med. Res. Rev.*, 2023, vol. 43, iss. 4, pp. 1141–1200. DOI: https://doi.org/10.1002/med.21948

[9] Suresh S. Biomechanics and biophysics of cancer cells. *Acta Biomater.*, 2007, vol. 3, iss. 4, pp. 413–438. DOI: https://doi.org/10.1016/j.actbio.2007.04.002

[10] Cross S.E., Jin Y.S., Rao J., et al. Nanomechanical analysis of cells from cancer patients. *Nature Nanotech.*, 2007, vol. 2, no. 12, pp. 780–783.
DOI: https://doi.org/10.1038/nnano.2007.388

[11] Daniel C., Traub F., Sachsenmaier S., et al. An exploratory study of cell stiffness as a mechanical label-free biomarker across multiple musculoskeletal sarcoma cells. *BMC Cancer*, 2023, vol. 23, art. 862. DOI: https://doi.org/10.1186/s12885-023-11375-3

[12] Guo X., Bonin K., Scarpinato K., et al. The effect of neighboring cells on the stiffness of cancerous and non-cancerous human mammary epithelial cells. *New J. Phys.*, 2014, vol. 16, art. 105002. DOI: https://doi.org/10.1088/1367-2630/16/10/105002

[13] Zhao Y., Ye X., Xiong Z., et al. Cancer metabolism: the role of ROS in DNA damage and induction of apoptosis in cancer cells. *Metabolites*, 2023 vol. 13, no. 7, art. 796.
DOI: https://doi.org/10.3390/metabo13070796

[14] Alloisio G., Rodriguez DB., Luce M., et al. Cyclic stretch-induced mechanical stress applied at 1 Hz frequency can alter the metastatic potential properties of SAOS-2 osteosarcoma cells. *Int. J. Mol. Sci.*, 2023, vol. 24, no. 9, art. 7686.
DOI: https://doi.org/10.3390/ijms24097686

[15] Walters B., Uynuk-Ool T., Rothdiener M., et al. Engineering the geometrical shape of mesenchymal stromal cells through defined cyclic stretch regimens. *Sci. Rep.*, 2017, vol. 7, art. 6640. DOI: https://doi.org/10.1038/s41598-017-06794-9

[16] Dhein S., Schreiber A., Steinbach S., et al. Mechanical control of cell biology. Effects of cyclic mechanical stretch on cardiomyocyte cellular organization. *Prog. Biophys. Mol. Biol.*, 2014, vol. 115, iss. 2-3, pp. 93–102.
DOI: https://doi.org/10.1016/j.pbiomolbio.2014.06.006

[17] Onal S., Alkaisi M.M., Nock V. Application of sequential cyclic compression on cancer cells in a flexible microdevice. *PLoS One*, 2023, vol. 18, art. e0279896.
DOI: https://doi.org/10.1371/journal.pone.0279896

[18] Wong A.K., Llanos P., Boroda N., et al. A parallel-plate flow chamber for mechanical characterization of endothelial cells exposed to laminar shear stress. *Cel. Mol. Bioeng.*, 2016, vol. 9, no. 1, pp. 127–138. DOI: https://doi.org/10.1007/s12195-015-0424-5

[19] Xin Y., Hu B., Li K., et al. Circulating tumor cells with metastasis-initiating competence survive fluid shear stress during hematogenous dissemination through CXCR4-PI3K/AKT signaling. *Cancer Lett.*, 2024, vol. 590, art. 216870.
DOI: https://doi.org/10.1016/j.canlet.2024.216870

[20] Po A., Giuliani A., Masiello M.G., et al. Phenotypic transitions enacted by simulated microgravity do not alter coherence in gene transcription profile. *npj Microgravity*, 2019, vol. 5, art. 27. DOI: https://doi.org/10.1038/s41526-019-0088-x

[21] Melica M.E., Cialdai F., La Regina G., et al. Modeled microgravity unravels the roles of mechanical forces in renal progenitor cell physiology. *Stem Cell Res. Ther.*, 2024, vol. 15, art. 20. DOI: https://doi.org/10.1186/s13287-024-03633-3

[22] Janmaleki M., Pachenari M., Seyedpour S.M., et al. Impact of simulated microgravity on cytoskeleton and viscoelastic properties of endothelial cell. *Sci. Rep.*, 2016, vol. 6, art. 32418. DOI: https://doi.org/10.1038/srep32418

[23] Espina J.A., Cordeiro M.H., Milivojevic M., et al. Response of cells and tissues to shear stress. *J. Cell Sci.*, 2023, vol. 136, no. 18, art. jcs260985.
DOI: https://doi.org/10.1242/jcs.260985

[24] Qiu Y., Gao T., Smith B.R. Mechanical deformation and death of circulating tumor cells in the bloodstream. *Cancer Metastasis Rev.*, 2024, vol. 43, no. 4, pp. 1489–1510. DOI: https://doi.org/10.1007/s10555-024-10198-3

[25] Kerdegari S., Canepa P., Odino D., et al. Insights in cell biomechanics through atomic force microscopy. *Materials*, 2023, vol. 16, no. 8, art. 2980.
DOI: https://doi.org/10.3390/ma16082980

[26] Zhou G., Zhang B., Tang G., et al. Cells nanomechanics by atomic force micr-scopy: focus on interactions at nanoscale. *Adv. Phys. X*, 2021, vol. 6, iss. 1, art. 1866668. DOI: https://doi.org/10.1080/23746149.2020.1866668

[27] Niu M., Luo G., Shu X., et al. Portable quantitative phase microscope for material metrology and biological imaging. *Photonics Res.*, 2020, vol. 8, iss. 7, art. 1253.
DOI: https://doi.org/10.1364/prj.396135

[28] Butt S.S., Fida I., Fatima M., et al. Quantitative phase imaging for characterization of single cell growth dynamics. *Lasers Med. Sci.*, 2023, vol. 38, art. 241.
DOI: https://doi.org/10.1007/s10103-023-03902-2

[29] Pirone D., Bianco V., Miccio L., et al. Beyond fluorescence: advances in computational label-free full specificity in 3D quantitative phase microscopy. *Curr. Opin. Biotechnol.*, 2024, vol. 85, art. 103054. DOI: https://doi.org/10.1016/j.copbio.2023.103054

[30] Branecka N., Lekszycki T. Experimental methods of living cells mechanical loading: review. *Contin. Mech. Thermodyn.*, 2023, vol. 35, no. 3, pp. 1165–1183. DOI: https://doi.org/10.1007/s00161-022-01099-3

[31] Moreno-Flores S., Benitez R., Vivanco M.D.M., et al. Stress relaxation and creep on living cells with the atomic force microscope: a means to calculate elastic moduli and viscosities of cell components. *Nanotechnology*, 2010, vol. 21, no. 44, art. 445101. DOI: https://doi.org/10.1088/0957-4484/21/44/445101

[32] Babahosseini H., Carmichael B., Strobl J.S., et al. Sub-cellular force microscopy in single normal and cancer cells. *Biochem. Biophys. Res. Commun.*, 2015, vol. 463, iss. 4, pp. 587–592. DOI: https://doi.org/10.1016/j.bbrc.2015.05.100

[33] Efremov Y.M., Okajima T., Raman A. Measuring viscoelasticity of soft biological samples using atomic force microscopy. *Soft Matter.*, 2020, vol. 16, no. 1, pp. 64–81. DOI: https://doi.org/10.1039/c9sm01020c

[34] Safa B.T., Huang C., Kabla A., et al. Active viscoelastic models for cell and tissue mechanics. *R. Soc. Open Sci.*, 2024, vol. 11, no. 4, art. 231074. DOI: https://doi.org/10.1098/rsos.231074

[35] Chang T.K., Rossikhin Y.A., Shitikova M.V., et al. Application of fractional-derivative standard linear solid model to impact response of human frontal bone. *Theor. Appl. Fract. Mech.*, 2011, vol. 56, no. 3, pp. 148–153. DOI: https://doi.org/10.1016/j.tafmec.2011.11.003

[36] De Sousa J.S., Freire R.S., Sousa F.D., et al. Double power-law viscoelastic relaxation of living cells encodes motility trends. *Sci. Rep.*, 2020, vol. 10, art. 4749. DOI: https://doi.org/10.1038/s41598-020-61631-w

[37] Carmichael B., Babahosseini H., Mahmoodi S.N., et al. The fractional viscoelastic response of human breast tissue cells. *Phys. Biol.*, 2015, vol. 12, no. 4, art. 046001. DOI: https://doi.org/10.1088/1478-3975/12/4/046001

[38] Bonfanti A., Kaplan J.L., Charras G., et al. Fractional viscoelastic models for power-law materials. *Soft Matter.*, 2020, vol. 16, no. 26, pp. 6002–6020. DOI: https://doi.org/10.1039/d0sm00354a

[39] Kang S., Yang X., Li Y., et al. A fractional viscoelastic mechanical model for speed optimization of robotic cell microinjection. *IEEE/ASME Trans. Mechatron.*, 2024, vol. 29, no. 6, pp. 4514–4525. DOI: https://doi.org/10.1109/TMECH.2024.3378908

[40] Fabry B., Maksym G.N., Butler J.P., et al. Scaling the microrheology of living cells. *Phys. Rev. Lett.*, 2001, vol. 87, no. 14, art. 148102. DOI: https://doi.org/10.1103/PhysRevLett.87.148102

[41] Sollich P., Lequeux F., Hébraud P., et al. Rheology of soft glassy materials. *Phys. Rev. Lett.*, 1997, vol. 78, no. 10, pp. 2020–2023.
DOI: https://doi.org/10.1103/PhysRevLett.78.2020

[42] Boocock D., Hirashima T., Hannezo E. Interplay between mechanochemical patterning and glassy dynamics in cellular monolayers. *PRX Life*, 2023, vol. 1, no. 1, art. 013001. DOI: https://doi.org/10.1103/prxlife.1.013001

[43] Grozdanov S., Lucas A., Poovuttikul N. Holography and hydrodynamics with weakly broken symmetries. *Phys. Rev. D*, 2019, vol. 99, no. 8, art. 086012.
DOI: https://doi.org/10.1103/PhysRevD.99.086012

[44] Fielding S.M. Elastoviscoplastic rheology and aging in a simplified soft glassy constitutive model. *J. Rheol.*, 2020, vol. 64, no. 3, pp. 723–738.
DOI: https://doi.org/10.1122/1.5140465

[45] Deshpande V.S., McMeeking R.M., Evans A.G. A bio-chemo-mechanical model for cell contractility. *Proc. Natl. Acad. Sci. USA*, 2006, vol. 103, no. 38, pp. 14015–14020. DOI: https://doi.org/10.1073/pnas.0605837103

[46] Mcgarry J.P., Fu J., Yang M.T., et al. Simulation of the contractile response of cells on an array of micro-posts. *Philos. Trans. A Math. Phys. Eng. Sci.*, 2009, vol. 367, iss. 1902, pp. 3477–3497. DOI: https://doi.org/10.1098/rsta.2009.0097

[47] Truong D., Bahls C.R., Nebe B., et al. Simulation of actin distribution of osteoblasts on titanium pillar arrays using a bio-chemo-mechanical model. *Int. J. Numer. Method Biomed. Eng.*, 2018, vol. 34, no. 8, art. e3097. DOI: https://doi.org/10.1002/cnm.3097

[48] Sun S.-Y., Zhang H., Fang W., et al. Bio-chemo-mechanical coupling models of soft biological materials: a review. In Bordas S.P.A. (ed.): *Advances in Applied Mechanics*, vol. 55. Elsevier, 2022, pp. 309–392.
DOI: https://doi.org/10.1016/bs.aams.2022.05.004

[49] Nikitiuk A.S., Koshkina A.A., Bayandin Y.V., et al. On thermodynamics and relaxation properties of eukaryotic cells. *Int. J. Non Linear Mech.*, 2023, vol. 157, art. 104532. DOI: https://doi.org/10.1016/j.ijnonlinmec.2023.104532

[50] Eldridge W.J., Sheinfeld A., Rinehart M.T., et al. Imaging deformation of adherent cells due to shear stress using quantitative phase imaging. *Opt. Lett.*, 2016, vol. 41, iss. 2, art. 352. DOI: https://doi.org/10.1364/ol.41.000352

[51] Landau L.D., Lifshitz E.M. Statistical physics. Pergamon Press, 1969.

[52] Eldridge W.J., Ceballos S., Shah T., et al. Shear modulus measurement by quantitative phase imaging and correlation with atomic force microscopy. *Biophys. J.*, 2019, vol. 117, iss. 4, pp. 696–705. DOI: https://doi.org/10.1016/j.bpj.2019.07.008

[53] Meidav T. Viscoelastic properties of the standard linear solid. *Geophys. Prospect.*, 1964, vol. 12, no. 1, pp. 80–99.
DOI: https://doi.org/10.1111/j.1365-2478.1964.tb01891.x

[54] Shliomos M.I., Raikher Y.L. Orientational ordering and mechanical properties of solid polymers. *Sov. Phys. JETP*, 1978, vol. 47, no. 5, pp. 1760–1783.

Knyazev N.A. — Post-Graduate Student, Engineer, Laboratory of Physical Foundations of Strength, ICMM UB RAS (Akademika Koroleva ul. 1, Perm, 614013 Russian Federation).

Nikityuk A.S. — Cand. Sc. (Phys.-Math.), Senior Research Scientist, Laboratory of Physical Foundations of Strength, ICMM UB RAS (Akademika Koroleva ul. 1, Perm, 614013 Russian Federation).

Please cite this article as:

Knyazev N.A., Nikityuk A.S. Nonlinear model for deformation of adherent cells due to shear stress. *Herald of the Bauman Moscow State Technical University, Series Natural Sciences*, 2026, no. 2 (125), pp. 20–40. EDN: TJDWYY